RL-TR-96-44
In-House Report
May 1996

GIGABIT OPTICAL INTERCONNECT TESTBEDS

Mark F. Krol, Raymond K. Boncek, Michael J. Hayduk,
and David J. Grucza

APPROVED FOR PUBLIC RELEASE; DISTRIBUTION UNLIMITED.

Rome Laboratory
Air Force Materiel Command
Rome, New York

This report has been reviewed by the Rome Laboratory Public Affairs Office (PA) and is releasable to the National Technical Information Service (NTIS). At NTIS it will be releasable to the general public, including foreign nations.

RL-TR-96-44 has been reviewed and is approved for publication.

APPROVED:

JAMES W. CUSACK, Chief
Photonics Division
Surveillance and Photonics Directorate

FOR THE COMMANDER:

DONALD W. HANSON, Director
Surveillance and Photonics Directorate

If your address has changed or if you wish to be removed from the Rome Laboratory mailing list, or if the addressee is no longer employed by your organization, please notify Rome Laboratory/OCPA, Rome, NY 13441. This will assist us in maintaining a current mailing list.

Do not return copies of this report unless contractual obligations or notices on a specific document require that it be returned.

REPORT DOCUMENTATION PAGE

Form Approved
OMB No. 0704-0188

1. AGENCY USE ONLY (Leave Blank)	2. REPORT DATE	3. REPORT TYPE AND DATES COVERED
	May 1996	In-House Oct 93 - Sep 95

4. TITLE AND SUBTITLE

GIGABIT OPTICAL INTERCONNECT TESTBEDS

5. FUNDING NUMBERS

PE - 62702F
PR - 4600
TA - P2
WU - 13

6. AUTHOR(S)

Mark F. Krol, Raymond K. Boncek, Michael J. Hayduk,
David J. Grucza

7. PERFORMING ORGANIZATION NAME(S) AND ADDRESS(ES)

Rome Laboratory/OCPA
25 Electronics Pky
Rome, NY 13441-4515

8. PERFORMING ORGANIZATION REPORT NUMBER

DL-6-0027

9. SPONSORING/MONITORING AGENCY NAME(S) AND ADDRESS(ES)

Rome Laboratory/OPCA
25 Electronic Pky
Rome, NY 13441-4515

10. SPONSORING/MONITORING AGENCY REPORT NUMBER

RL-TR-96-44

11. SUPPLEMENTARY NOTES

Rome Laboratory Project Engineer: Raymond K. Boncek, RL/OPCA, (315)330-2937

12a. DISTRIBUTION/AVAILABILITY STATEMENT

Approved for public release; distribution unlimited.

12b. DISTRIBUTION CODE

13. ABSTRACT (Maximum 200 words)

This report describes the results of experiments performed in various areas of material and component technology required for the development of gigabit optical interconnect and communication systems. First, we will summarize the analysis of transient and optoelectronic feedback-sustained pulsation of laser diodes at 1300 nm for use as frequency variable sources in time-division optical systems. Next, we describe the design and characterization of a colliding pulse Mach-Zehnder modulator capable of performing all-optical demultiplexing at data rates approaching 100 Gbps. Then, we comment on the investigation of ultrafast electron and hole tunneling in ternary asymmetric double quantum wells which may be suitable materials for use in future fiber-based communication systems. Finally, we report on the development of a low-voltage real-space electron transfer modulator for use in high-speed opto-electronic systems. This work is a continuation of in-house efforts begun under 62702F, JON 4600P206, and summarized in RL-TR-94-86.

14. SUBJECT TERMS	15. NUMBER OF PAGES
asymmetric coupled quantum wells, optical fiber, interconnect networks, modulators, semiconductor, All-optical, Mach-Zehnder, self-pulsation, charge transfer	44
	16. PRICE CODE

17. SECURITY CLASSIFICATION OF REPORT	18. SECURITY CLASSIFICATION OF THIS PAGE	19. SECURITY CLASSIFICATION OF ABSTRACT	20. LIMITATION OF ABSTRACT
UNCLASSIFIED	UNCLASSIFIED	UNCLASSIFIED	U/L

Table of Contents

Section		Page
1.	Introduction	1
2,	Transient and Optoelectronic Feedback-Sustained Pulsation of Laser Diodes at 1300 nm	2
3.	Colliding Pulse Mach-Zehnder Modulator	9
4.	Tunneling and Asymmetric Coupled Quantum Well Structures	11
5.	Charge Transfer Optical Modulator	20
6.	References	30
7.	Acknowledgment	34

1. Introduction

Optical interconnects are a means of alleviating the electronic input/output (I/O) bottleneck inherent in ultra-fast communication systems. With the development of multi-gigahertz bandwidth optical interconnects as our goal, we have undertaken efforts to develop promising technology for use in fulfilling the physical-layer requirements of ultra-fast communication systems. The investigation of these technologies, such as self-sustained pulsation of semiconductor laser diodes, colliding pulse mach-Zehnder optical demultiplexers, tunneling and asymmetric quantum well materials for electro-optical modulators and charge transfer devices are a direct result of previous work on testbed characterization and performance analysis. The results of this work indicated that off-the-shelf components have deficiencies associated with their application in gigabit optical interconnects. Thus, development of materials and components which overcome these performance deficiencies is an ongoing major thrust of our experimental work.

The work performed in the current work unit can be summarized by four major efforts as follows.

1. The investigation of the phenomena of self-sustained, transient self-, and feedback sustained pulsation in semiconductor laser diodes at 780, 850 and 1300 nm for use in antenna remoting and local network applications [1].
2. Development of a colliding-pulse Mach-Zehnder optical demultiplexer for use in ultra-fast time-domain multiplexed interconnects [2].
3. Tunneling and asymmetric coupled quantum well structures for use in ultra-fast electro-optical modulators [3].
4. Charge transfer optical modulators which significantly reduce the applied bias voltage requirements while maintaining the modulation bandwidth requirements of terahertz optical interconnects [4].

Each of these efforts has resulted in a significant contribution to the development and design of multi-gigahertz bandwidth optical interconnects. It is also interesting to note that these materials and components are not solely limited toward application in time-division-multiplexed, optical fiber

interconnects. Indeed, many of the results reported here are applicable to analog optical interconnects as well.

2. Transient and Optoelectronic Feedback-Sustained Pulsation of Laser Diodes at 1300 nm

Self-sustained pulsation (SSP) is a well-known dynamic process in laser diodes [5]. It has been extensively studied both experimentally and theoretically [6,7,8]. The majority of these previous experiments has been conducted in 780 nm laser diodes. SSP was first considered to be a nuisance and there were efforts aimed at reducing or eliminating SSP. It was realized later on that SSP laser diodes have low relative intensity noise (RIN) because of short coherence length which reduced the effects of optical feedback into the laser diodes. SSP laser diodes have also been proposed for use in all-optical clock recovery [9]. Recently, a promising new application has emerged in which SSP would be used as subcarriers for lightwave communication networks [10]. Both analog (up to 1 GHz) [11] and digital (up to 800 Mb/s) [12,13] transmission using SSP subcarriers have been reported. Subcarrier-multiplexing (SCM) not only is compatible with wavelength-division multiplexing (WDM) but also can extend the capacity of WDM networks [14]. As a result, WDM-SCM networks are of particular interest for local area networks (LAN) where pure WDM may not be able to provide a large number of nodes. It is therefore important to generate microwave subcarriers in laser diodes at wavelengths other than 780 nm. This letter describes SSP, transient self-pulsation (TSP), and the generation and frequency modulation of feedback-sustained pulsations (FSP) in laser diodes at 1300 nm.

The schematic of the experimental setup is shown in Figure 1. The pulsations were observed in Mitsubishi Electric ML7011R InGaAsP single-mode (pigtailed) laser diodes (LD). The emission wavelength of these laser diodes is near 1300 nm with typical fiber-coupled CW output powers of 0.5 mW. The laser diode is temperature stabilized to using a thermal electric cooler (TEC). The pigtailed fiber from the laser diode is fusion spliced to a 3 dB bi-directional fiber

coupler. Half of the laser output was used for monitoring the optical spectrum using an Anritsu MS9001B1 optical spectrum analyzer (OSA). The other half of the laser output was used for feedback into the laser diode through an optoelectronic feedback loop. The first component in the optoelectronic feedback loop is a photodetector (PD) which converts laser light pulsations into microwave oscillations. The microwave signal is pre-amplified using a Miteq 18-GHz wideband low-noise amplifier. The amplified signal is split into two parts using an rf power splitter. Half of the rf power was used for monitoring the spectrum of the microwave oscillations using a HP 8593E microwave spectrum analyzer. The second half of the pre-amplified signal was fed into the laser diode through the ac port of the bias tee via a bandpass filter (BPF), another wideband amplifier and a microwave power combiner (COM). The other input port of the COM was used for modulating signals.

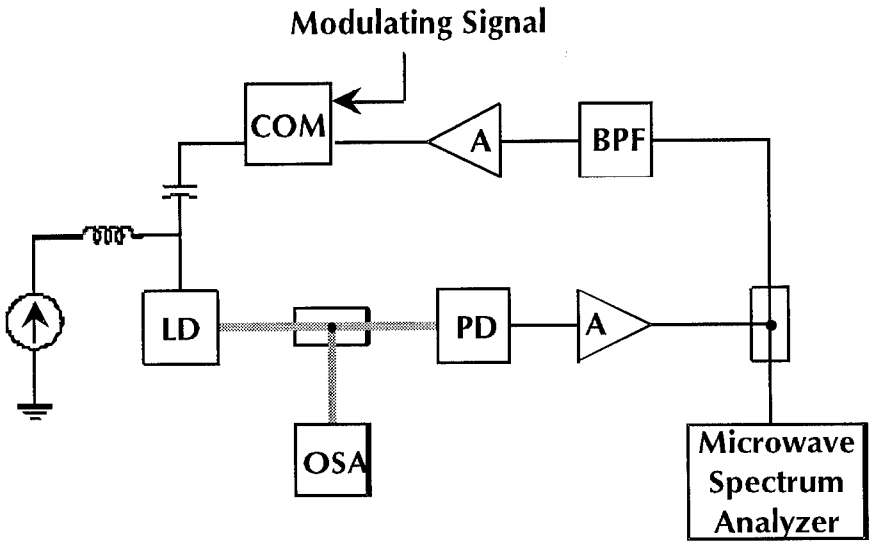

Figure 1. Schematic of the experimental setup for studying SSP, TSP and FSP.

Self-pulsations in the laser diodes (with the feedback being turned off) fall into two categories, SSP and TSP. The laser intensity pulsations observed in this experiment are predominantly transient in nature. SSP only occurs within a very small range of bias current. The frequency

range of the self-pulsation is between 2.0 GHz to 7.0 GHz. All laser diodes we have examined showed qualitatively similar pulsation behavior. For example, a particular laser diode exhibited self pulsation for bias currents between 17.0 and 32.0 mA with pulsation frequencies ranging from 3.5 GHz to 6.5 GHz. However, SSP only occurs for bias current values near 20 mA. Self-pulsations for other bias current were transient in nature. In Transient self-pulsations (TSP), the intensity pulsation occurred as soon as the laser diode was turned on or turned to a different bias current but then experienced a continued decay in intensity. TSP typically only lasted for 1 to 3 minutes. Fig. 2 shows the microwave spectra of TSP with a bias current of 21.0 mA. The top trace (thin line) is the spectrum of TSP immediately after the laser diode was turned on and the lower trace (thick line) is the spectrum of TSP 35 seconds later. The magnitude of the self-pulsation reduced significantly in 35 seconds. The TSP disappeared in about 45 seconds. The (FWHM) linewidth of the TSP is very broad and is on the order of 0.5 GHz. The microwave spectra of the SSP (at a bias current near 20 mA) are not shown here but are very similar to that of the top trace in Fig.2 except they are shifted to lower frequencies.

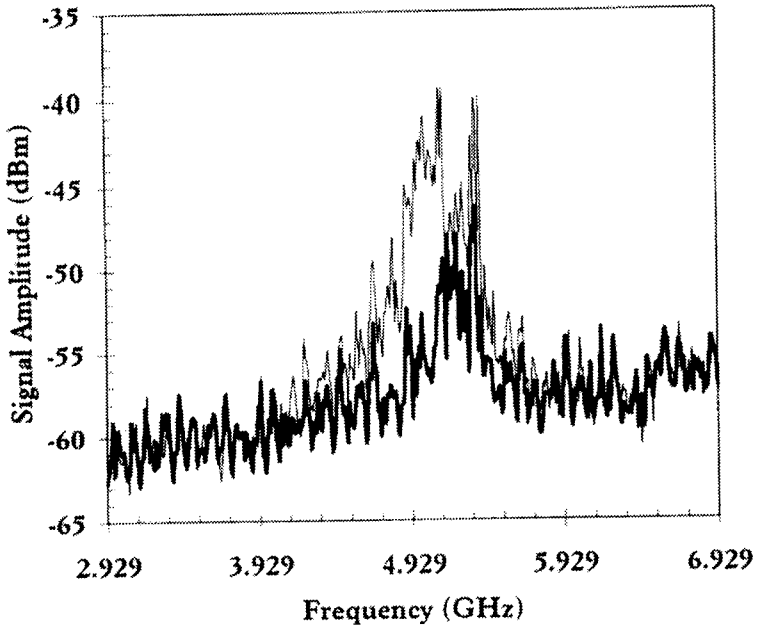

Figure 2 Microwave spectra of TSP at a bias current of 21 mA immediately after turn on (top, thin trace) and 35 seconds after turn on (lower, thick trace).

Optoelectronic feedback has been used in previous work to reduce the linewidth of SSP [10,11]. In this work, optoelectronic feedback was used to stabilize the TSP producing feedback-sustained pulsation (FSP). Furthermore, the linewidth of FSP was also significantly reduced compared to that of the TSP. The center frequency of the FSP was determined by the passband of the bandpass filter and can therefore be tuned by the BPF. In addition, the frequency of FSP with a fixed BPF can be fine tuned by laser diode bias current. This fine-tuning range was about 45 MHz. Along with the generation of FSP with optoelectronic feedback were changes in the optical spectrum of the laser light.

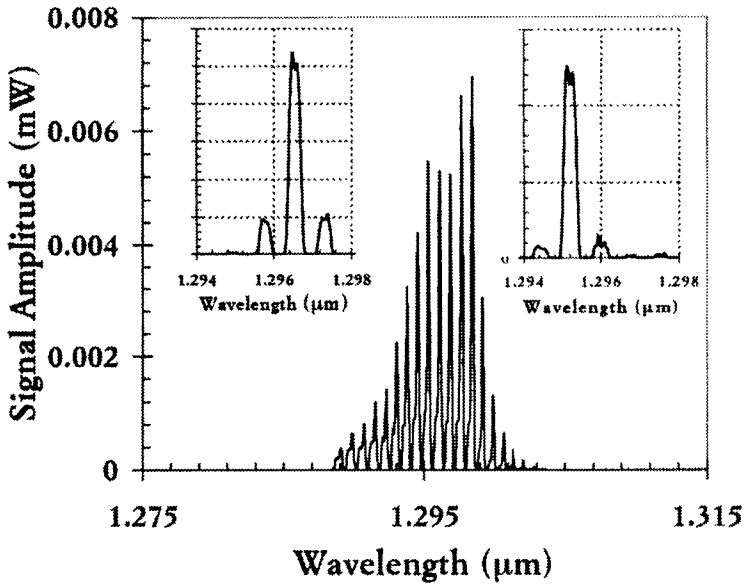

Figure 3 Optical spectra of laser output for (a) free running condition (upper-left inset), (b) weak optoelectronic feedback (main plot), and (c) strong optoelectronic feedback (upper-right inset).

The laser diodes used in this experiment are single mode. The spectrum of a free running laser diode is shown in the upper-left inset in Fig. 3. There are not noticeable differences in the optical spectra for TSP and SSP regions of free-running operation. In this particular spectrum the two side modes were about 7 dB down from the main mode. Almost all the optical power was

contained in a wavelength span of about 2.0 nm. Optoelectronic feedback significantly affects the optical spectrum of the laser diode output. The main plot in Fig. 3 is the optical spectrum of the laser output when the feedback was slightly above a threshold value for stable FSP. Now the wavelength span is about 15 nm. This result is very similar to the coherence collapse observed in laser diodes with external optical feedback [15]. As the feedback was increased beyond a critical value, the optical spectrum, shown in upper-right inset in Fig. 3, switched into a form that more resembled that of the free running laser diode except for a few additional, very weak side modes. The entire spectrum also shifted towards shorter wavelength by 1 nm. It is worth mentioning that "strong" and "weak" feedback here are only qualitatively defined since the bias tee is not broadly matched to the laser diode and, as a result, it was not possible to easily estimate the extent of reflection of the feedback signal.

Now we present the electrical characteristics of the FSP. As mentioned earlier, the frequency of the FSP is predominantly determined by the passband of the bandpass filter. With a fixed BPF of center frequency 4.76 GHz, 10% -3 dB passband and 20% passband at -30 dB, the microwave spectrum of the FSP is shown in Fig. 4. The fundamental frequency of the FSP is 4.70 GHz. High-order harmonics are also present in the FSP signal but are of lower amplitudes. The second harmonic is 20 dB below the fundamental harmonic. The linewidth of the fundamental FSP peak is very narrow, about 20 kHz, as shown in inset to Fig. 4.

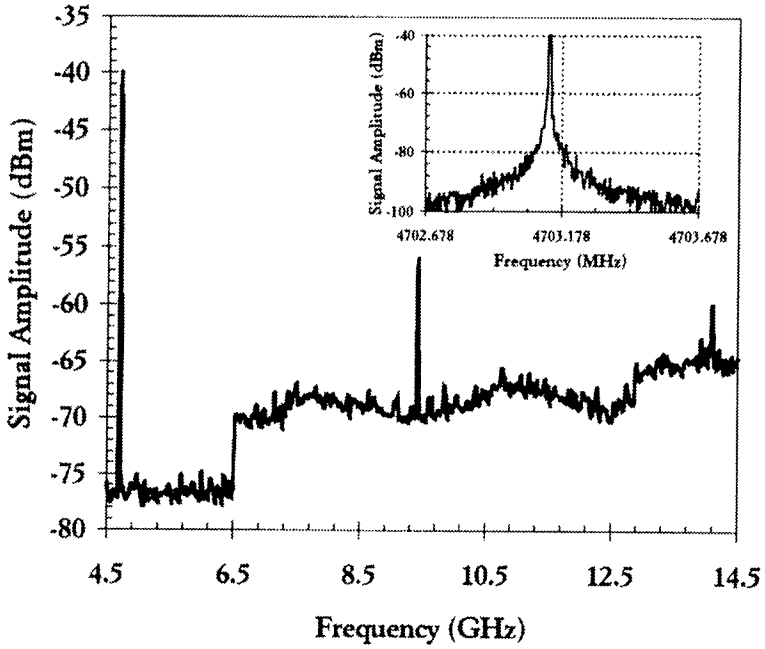

Figure 4 Microwave spectrum of a FSP signal with all harmonics included. The inset is the fundamental harmonic only.

When an rf signal is applied to the laser diode (see Fig. 1), the frequency of FSP is modulated by the applied rf signal. Figure 5 shows the spectrum of the frequency-modulated FSP signal. The carrier is the 2.88885 GHz FSP (with a 2.90 GHz bandpass filter) and the modulating signal is a 20 MHz sinusoid. Four sidebands are observed. The uneven first sidebands signifies residual amplitude modulation in the FM signal. This is expected because the laser output power is also dependent on the bias current. Frequency modulation of FSP by signals of frequencies exceeding 500 MHz have been demonstrated in the experiment. This FM signal can be demodulated using standard FM demodulators such as the delay line demodulator. We have achieved a signal-to-noise ratio of about 25 dB. The details of communication links and networks using FSP will be presented elsewhere.

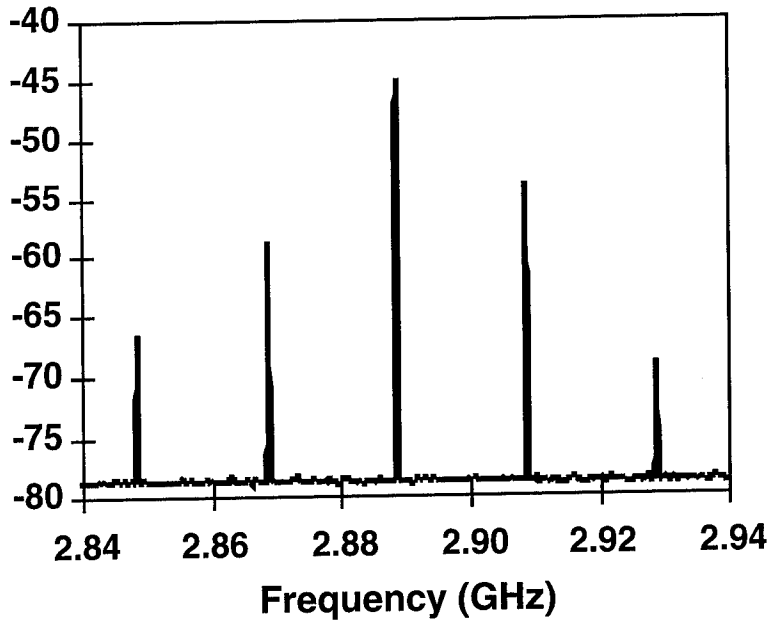

Figure 5. Microwave spectrum of a 2.88885 GHz FSP frequency modulated by a 20 MHz sinusoidal signal.

In conclusion, we report the observation of self-sustained pulsation and transient self-pulsation in 1300 nm laser diodes. The mechanism for SSP is generally believed to be the formation of periodic orbits due to Hopf bifurcation in the laser diode nonlinear dynamics [10]. Transient self-pulsations have not been reported before. The origin of TSP is still under investigation. Although TSP is similar to the relaxation oscillation [16], the transient time of minutes for TSP is much longer than typical relaxation oscillation time. With optoelectronic feedback, TSP and SSP turn into stable FSP which can be used as high-frequency tunable microwave subcarriers at 1300 nm. For WDM-SCM applications, it is important to provide sufficient optoelectronic feedback so that the optical spectrum of the laser output remains narrow. Even though FSP can be frequency modulated by very high-frequency signals (>500 MHz), the peak frequency deviation is within 45 MHz. We are currently investigating methods for achieving larger peak frequency deviation/modulation index for improved signal-to-noise ratios.

3. Colliding Pulse Mach-Zehnder Modulator

Recently developed ultra-fast optical switches based on the Sagnac and Mach-Zehnder interferometric principle have been demonstrated for use in ultra-fast optical time-domain multiplexed (OTDM) interconnects [17]. Using resonant optical nonlinearities, such switches have demonstrated switching windows of a few picosecond in duration while requiring small optical control pulse energies [18,19]. For ultra-fast switches based on the Mach-Zehnder, there are two additional configurations possible with different propagation geometries for the control and data pulses. Each geometry has it's own advantages and disadvantages for the future implementation in OTDM systems.

The colliding pulse Mach-Zehnder configuration has demonstrated 10 ps switching window using only 650 fJ of control pulse energy [2]. Compared to the previously demonstrated system [19] with a co-propagation geometry of the control and data pulses in the Mach-Zehnder, the colliding pulse geometry uses counter propagation control and data pulses. The counter propagating geometry does not require any optical components to reject the high optical control pulse from the weak data pulse. The utilized optical nonlinearity is based on gain compression in a semiconductor optical amplifier [18], so the device will permit signal fanout and thus cascadability.

The switch is constructed with passive fiber optic components and two semiconductor optical amplifiers (SOAs) (500 μm long InGaAsP) as shown in Figure 6 [2]. The control and data pulses are 2 ps in duration and counter propagate in the arms of the Mach-Zehnder The different arrival times of the control and data pulses on the asymmetrically placed SOAs determine the ultra-fast switching window. The constructed Mach-Zehnder has been dynamically stabilized by adjusting the optical path length in one arm of the interferometer. Loop polarizers and the adjustable time delays provide the optimum condition for maximum interference of the output signal.

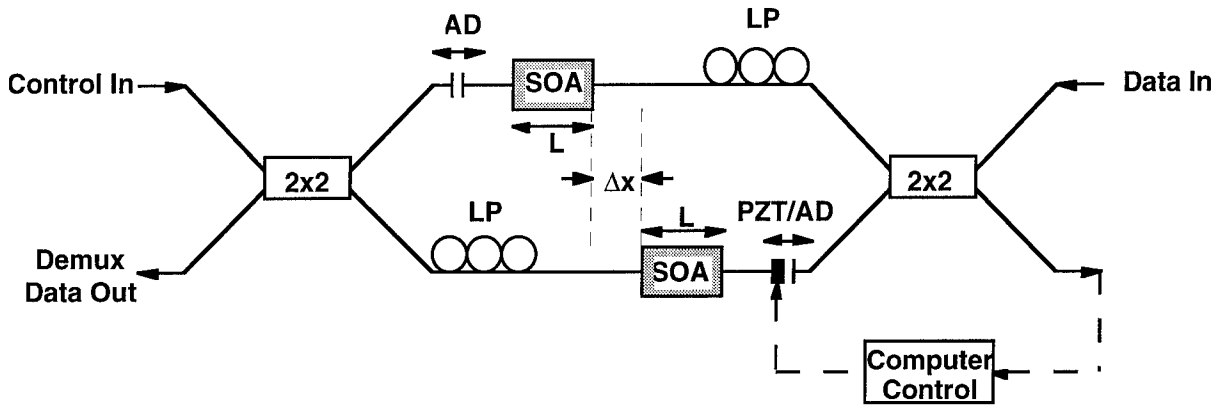

Figure 6. Colliding pulse Mach-Zehnder experimental setup. Component abbreviations, AD-adjustable delay, LP-loop polarization controller, SOA-semiconductor optical amplifier, PZT-piezo electric transducer, 2x2-bi-directional fiber optic coupler, L-length of SOA, Δx-SOA offset.

The experimental result showing a 10 ps switching window is illustrated in Figure 7. This data has been obtained by time delaying the control pulse with respect to the data pulse before propagating inside the Mach-Zehnder, similar to a time-domain spectroscopy or pump-probe measurement technique. The measured control and data pulses are at 1.313 μm originating from a mode-locked and pulse compressed Nd:YLF laser. The polarization state of the control and signal pulses do not need to be orthogonal to each other. With a similar experimental condition for the 20 ps switching window, 0.8π and 0.5π of nonlinear phase shifts have been estimated for each SOA [20].

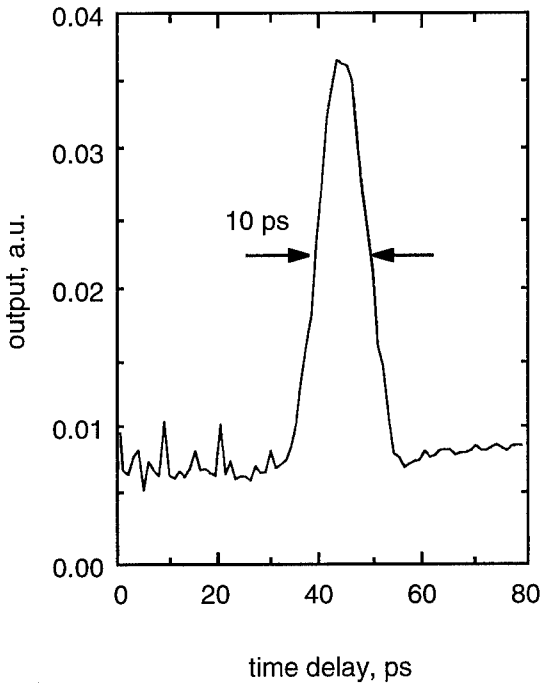

Figure 7. Measured 10 ps switching window.

Thus, this device has demonstrated a 10 ps switching window using only 650 fJ of control pulse energy. Special requirements to reject the control pulse energy are not required for this geometry, and therefore the wavelength of the control and data pulses can be identical unlike the copropagating geometry [19] and without the requirement of orthogonal polarization [18]. Other additional advantages of the device are its cascadability, fanout capability and the potential for small scale integration.

4. Tunneling and Asymmetric Coupled Quantum Well Structures

Tunneling in semiconductor heterostructures has been the topic of considerable research interest in recent years. In particular, electron and hole tunneling in Asymmetric Double Quantum Wells (ADQWs) has received much attention for ultrafast optical and optoelectronic device applications. Most research efforts have concentrated on the carrier dynamics in the

GaAs/(Ga,Al)As system.[21] However, very few studies have investigated carrier dynamics in ternary ADQW systems which are compatible with the optical fiber transmission windows of 1.3 and 1.5 μm.[22] It has been noted that electrons may tunnel rapidly via longitudinal optical (LO) phonon scattering when the energy separation between the lowest energy level in the narrow well (NW) and the lowest energy level in the wide well (WW) is larger than the LO phonon energy.[23-25] Fast hole tunneling between the NW and WW may also occur when there are resonances between hole subbands due to the presence of an applied electric field [26,27] or due to valence band mixing between NW and WW subbands.[28]

In this report, we present the first experimental evidence for ultrafast electron *and* hole tunneling in (Ga,In)As/(Al,In)As ADQW structures. These materials are compatible with optical fiber based applications where ultrafast optical and optoelectronic devices are required.[4] The study utilized a novel nondegenerate, transmission pump/probe technique. Two distinct carrier density dependent regimes were observed. A single tunneling time is observed at low carrier densities indicating the holes tunnel from the NW to the WW at least as fast as electrons.. At high carrier densities, however, a two component decay is observed, consistent with phase-space filling and space-charge effects blocking tunneling carriers.

The ADQW samples studied consisted of 30 periods of the following structure: 40 Å $Ga_{0.47}In_{0.53}As$ well/ L_b Å $Al_{0.48}In_{0.52}As$ tunnel barrier/ 60 Å $Ga_{0.47}In_{0.53}As$ well/ 100 Å $Al_{0.48}In_{0.52}As$ barrier, where L_b is the thickness of the tunnel barrier. These structures were grown by solid-source molecular beam epitaxy on semi-insulating (100) InP substrates. Three samples were studied with barrier widths of L_b = 27, 37, and 100 Å, denoted later as 40/L_b/60. The samples were of high optical quality as indicated by low temperature linear absorption (see inset of Fig. 1(b)) and photoluminescence measurements. At a sample temperature of 77 K the NW and WW heavy-hole exciton transition wavelengths were near 1.23 μm and 1.34 μm, respectively. The sample with the 100 Å barrier has essentially decoupled wells and experimentally shows no effects

due to tunneling. The ADQW samples were designed such that the energy separation between the lowest energy levels in the WW and NW was approximately 61 meV (the separation increased slightly as the barrier width was decreased). A large separation between the levels was chosen for two reasons: first, for energy separations less than 50 meV the calculated tunneling times were sub-picosecond making the pump induced transmission changes difficult to observe experimentally; and second, the separation between the levels is far from being in resonance with the LO phonon energy hence avoiding any significant change in the electron tunneling time due to space-charge induced level shifts.[29]

The experimental system used to measure the carrier dynamics utilized a novel time-resolved transmission/upconversion technique. In most previous studies of carrier dynamics in ADQWs time-resolved photoluminescence (PL) was utilized. In time-resolved PL, the product $f_e f_h$ is measured, where f_e and f_h are the Fermi distributions of the electrons and holes, respectively. Hence, if one type of carrier is absent the total signal is zero despite the existence of the other carrier. On the other hand, transmission techniques measure $1-f_e-f_h$. Therefore, the dynamics of the individual carriers change the transmission signal independently. In our approach, 100 fs pulses at 850 nm from a Kerr lens modelocked Ti:Sapphire laser were used to pump the samples and provide reference pulses for the upconversion process. The photon energy of the pump was tuned to generate carriers only in the wells, not in the barriers, with most of the excess energy carried by the electrons. A continuous wave Cr:Forsterite laser provided a tunable probe from 1.22 to 1.29 μm. The probe laser was tuned to the heavy-hole exciton absorption resonance of the NW for all measurements discussed in this paper (see inset of Fig. 1(b)). The samples were held at 77 K in a liquid nitrogen cryostat. The transmitted probe was mixed with the reference pulses in a 2 mm thick $LiIO_3$ crystal to provide femtosecond time-resolution. The temporal-resolution of the system was 220 fs and was limited by the group-velocity mismatch between the reference and probe in the nonlinear crystal.[30] The upconverted photons were spectrally filtered then detected

by a photomultiplier tube. The pump was chopped to measure the pump induced changes in the transmitted probe using lock-in detection.

The time-resolved transmission data for sample 40/27/60 is shown in Fig. 8(a) for a carrier density of $1.4\text{x}10^{11}$ cm^{-2}. Of these carriers approximately 3.5×10^{10} cm^{-2} were generated in the NW with the remaining 1.05×10^{11} cm^{-2} being generated in the WW. The difference in carrier densities between the two wells stems from the larger WW width (1.5 times larger than the NW) and the existence of two allowed WW interband transitions at the pump energy as opposed to one in the NW. The initial rise shows the relaxation of carriers to the bottom of the NW band. The subsequent decay is due to tunneling of carriers from the NW to the WW. The most striking feature in this data is the fast and full recovery of the transmission at this carrier density. The decay was fitted to a *single* exponential decay constant of 2.4 ps. The transmission fully recovers with a single time constant despite the fact that the probe wavelength was tuned to the heavy-hole exciton absorption peak of the NW. Since the upconversion technique measures $1-f_e-f_h$, full recovery indicates the absence of both electron and hole populations. To verify that the fast component of the decay was associated with the tunneling of carriers from the NW to the WW, the same measurement was performed using sample 40/37/60. The measured differential transmission signal is shown in Fig. 8(b). The time-constant associated with the decay was 11.5 ps. The results are consistent with tunneling phenomena, *i.e.* for a thicker barrier the time-constant of the fast component becomes longer. Sample 40/100/60 showed no recovery over our delay range, consistent with an essentially decoupled pair of wells.

To understand the dynamics observed in this work, we considered the electron behavior independently of the holes. Since the inter-well dynamics are not significantly affected by excitonic effects [31], we have neglected the coulomb attraction between electrons and holes in the following calculations. To treat the electron/LO phonon interaction in the ADQW structures we

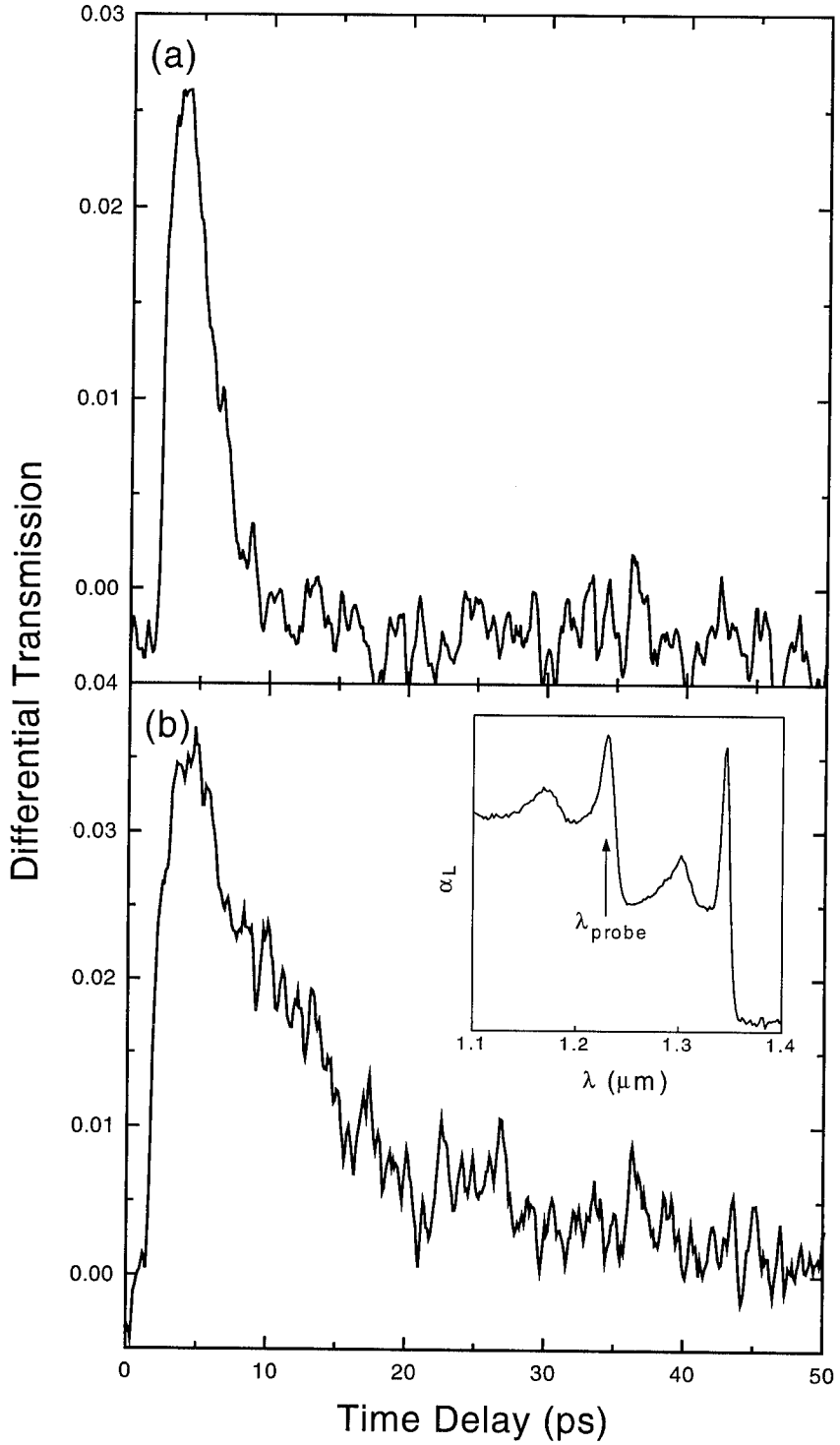

Figure 8 (a) Time-resolved differential transmission data for samples (a) 40/27/60 and (b) 40/37/60.

used Fermi's Golden Rule and the Fröhlich electron/LO phonon interaction potential. Additionally, the phonons were treated as bulk modes.[32] Under these assumptions, the following expression for the LO phonon assisted electron tunneling rate can be found:

$$\left(\frac{1}{\tau}\right)_{LO} = \frac{m^* e^2 \omega_{LO}}{\hbar^2}\left(\frac{1}{\kappa_\infty} - \frac{1}{\kappa_o}\right)\frac{1}{2\pi}\int_0^{2\pi}\left[(N+1)I^-(Q) + NI^+(Q)\right]d\theta \qquad (1)$$

where

$$I^{\pm}(Q) = \frac{\pi}{Q}\iint \chi_k(z)\chi_{k'}(z)\exp\left(-Q|z-z'|\right)\chi_k(z')\chi_{k'}(z')dz'dz \qquad (2)$$

In Eq.1, ω_{LO} is the angular frequency of the LO-phonon, e is the electronic charge, κ_o and κ_∞ are the static and dynamic dielectric constants of the crystal, respectively, m* is the electron effective mass, $Q=(k^2+k'^2-2kk'\cos\theta)^{1/2}$ is the magnitude of the in-plane momentum change, N is the phonon occupation number, and $\chi_k(z)$ and $\chi_{k'}(z)$ are the initial and final state electron envelope wavefunctions in the growth direction, respectively. The LO phonon energy for the $Ga_{0.47}In_{0.53}As$ well material was assumed to be 33.2 meV.[33] The +/- sign in Eq. 2 corresponds to phonon absorption or emission respectively. The affect of alloy scattering was also considered theoretically. However, the calculated tunneling times were two orders of magnitude longer than the phonon assisted tunneling times. The calculated barrier width dependence of the LO phonon assisted electron tunneling time at low carrier densities is shown in Fig. 9. Also shown in the figure are the measured time-constants for samples 40/27/60 and 40/37/60. The calculated electron tunneling times for these two samples are 2.2 and 10.5 ps, respectively. These times are in good agreement with the measured low density decay times. Thus, the transmission *fully recovers* with a time constant equal to the electron tunneling time. The good agreement between the observed fast recovery and the calculated electron tunneling time indicates that at low carrier densities the holes must tunnel as fast, or faster than the electrons.

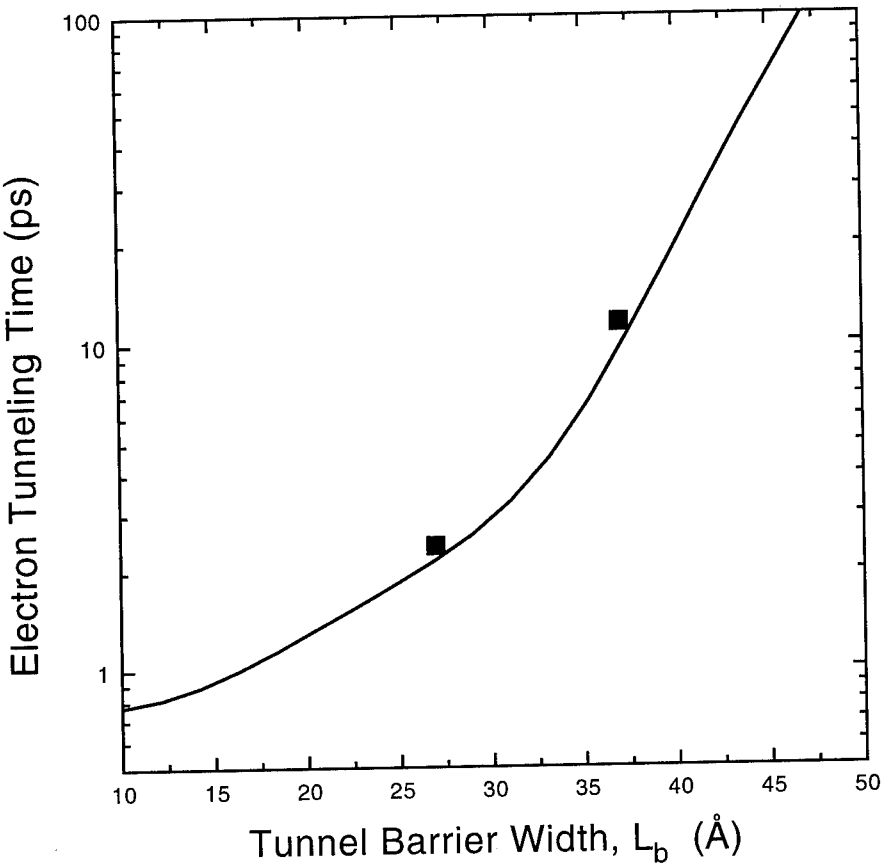

Figure 9 Calculated tunnel barrier width dependence of the electron tunneling time at low carrier densities (solid line). The measured low carrier density tunneling time-constants for samples 40/27/60 and 40/37/60 are also shown (squares).

The good agreement between the observed fast recovery and the calculated electron tunneling times provides strong evidence that at low carrier densities the observed transmission changes are due to only electrons arriving at the Γ point. In previous transmission studies of carrier dynamics in GaAs/(Al,Ga)As ADQWs, a long lasting component was observed for all carrier densities considered and was attributed to the relatively long time heavy-holes spend in the

NW due to their highly localized wavefunctions at the Γ point.[34,35] In both of these reports, however, the experiments used degenerate or nearly degenerate pump/probe techniques. Hence, holes are generated at or near the Γ point of the lowest heavy-hole subband of the NW. Our experimental technique is highly non-degenerate, and as a result, carriers are generated in the bands of interest with significant excess energy and in-plane momenta by the pump pulse, i.e. at $k \approx 0.05$ $Å^{-1}$. Thus, it is possible for holes generated in the NW to tunnel to the WW before reaching the Γ point of the NW.

Figure 10 shows the time-resolved differential transmission signal for sample 40/27/60 at carrier densities of $5.6x10^{11}$, $1.1x10^{12}$, and $2.3x10^{12}$ cm^{-2}. For carrier densities above $5.6x10^{11}$ cm^{-2}, a striking change in the differential transmission signal is observed. A long-lasting component appears which we attribute to holes arriving at the Γ point of the first NW heavy-hole subband. At low carrier densities, holes can efficiently tunnel from the NW to the WW during the relaxation process. Efficient tunneling can occur since away from the Γ point the NW and WW valence subbands are strongly mixed due to spin-orbit and band coupling.[28] However, at high carrier densities phase-space filling in the WW blocks tunneling holes and results in holes relaxing to the Γ point of the first NW heavy-hole subband. Another factor which may contribute to the generation of the long-lasting component is the build-up of space-charge induced fields due to the spatial separation of electrons and holes during the relaxation process. The fields can cause level shifts which can cause the rapid transfer of holes back to the NW.[26,29]

In summary, we have presented experimental evidence for ultrafast electron *and* hole tunneling in ternary ADQWs. Two distinct regimes were observed. First, at low carrier densities the differential transmission signal was found to recover with a time-constant equal to the LO phonon assisted electron tunneling time. The low density dynamics indicate that holes tunnel to the

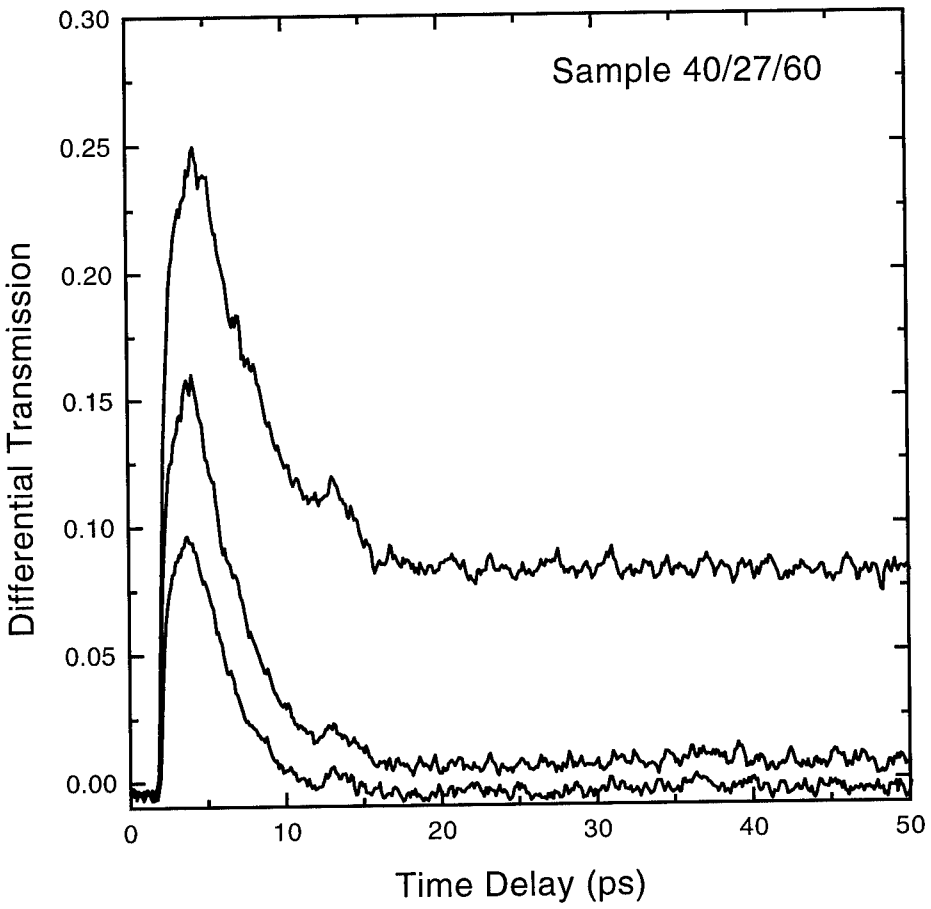

Figure 10 Time-resolved differential transmission data for sample 40/27/60 at carrier densities of 5.6×10^{11}, 1.1×10^{12}, and 2.3×10^{12} cm^{-2}, respectively.

WW before reaching the bottom of the NW and the observed transmission changes are due to electrons only. Second, at high carrier densities a long-lasting component was observed in the differential transmission signal which we attribute to the holes relaxing to the NW due to phase-space filling in the WW and space-charge effects. The experimental results presented here represent, to the best of our knowledge, the first observation of hole tunneling times which are at

least as fast as electron tunneling times. A detailed theoretical investigation of hole tunneling will be published elsewhere.

5. Charge Transfer Optical Modulator

For material systems such as (Ga,In)As/(Al,In)As quantum wells lattice matched to InP which are compatible with the optical fiber transmission windows of 1.3 and 1.5 μm, the quantum confined Stark effect (QCSE) is small due to the relatively low electron and heavy-hole effective masses and the restriction on suitable well widths, i.e. 40 and 85 Å, respectively. The use of electron transfer between a quaternary reservoir and single quantum well and the use of coupled quantum wells have been shown to be attractive alternatives for optical fiber compatible device applications.[36-38] Additionally, a large field-induced blue-shift of the heavy-hole exciton absorption resonance has been observed in narrow GaAs/(Al,Ga)As asymmetric coupled quantum wells near the heavy-hole resonance.[39] Although recent results utilizing the (Ga,Al,In)As/(Al,In)As on InP system have demonstrated improved material quality and device performance at these wavelengths[40-42], improvements in the electro-optic characteristics of these materials is still required. In this paper, a novel electroabsorption mechanism based on selective doping of (Ga,In)As/(Al,In)As asymmetric double quantum wells (ADQWs) is demonstrated.[4] The modulator utilizes real space transfer of excess electrons to provide efficient absorption modulation. The results are compared to absorption changes in an undoped ADQW structure

To study the real-space transfer of electrons in (Ga,In)As/(Al,In)As ADQWs, a sample was grown by molecular beam epitaxy on an *n*-type (100) InP substrate. The electrical bias was applied via a *p-i-n* mesa diode consisting of a 0.35 μm layer of *n*-type $Al_{0.48}In_{0.52}As$ (Si, 2×10^{18} cm^{-3}) followed by a 1.035 μm intrinsic region and capped with a 0.2 μm layer of *p*-type

$Al_{0.48}In_{0.52}As$ (Be, 2×10^{18} cm^{-3}) and a 200 Å *p*+ $Ga_{0.47}In_{0.53}As$ contact layer. The intrinsic region consisted of 30 periods of 100 Å $Al_{0.48}In_{0.52}As$ barrier/ 70 Å $Ga_{0.47}In_{0.53}As$ wide well/ 35 Å $Al_{0.48}In_{0.52}As$ tunnel barrier/ 40 Å $Ga_{0.47}In_{0.53}As$ narrow well all between two layers of 0.15 μm undoped $Al_{0.48}In_{0.52}As$. This ADQW structure is ideal for studying charge transfer since the ADQWs where designed to have the narrow well (NW) closer to the *n*-doped side of the *p-i-n* diode. The wide well (WW), on the other hand, is closer to the *p*-doped side of the diode. The orientation of the ADQWs allows electrons initially generated in the WW to transfer to the NW as a reverse bias is applied to the diode. The application of a reverse bias is critical for eliminating unwanted current flow through the diode.

To study the steady-state electron transfer process in ADQWs, time-integrated photoluminescence (PL) spectroscopy was utilized. Although time-integrated PL is a common technique, the experimental arrangement used here is unique in the fact that we used a continuous-wave Cr:Forsterite laser as the pump source. The Forsterite laser offers the capability to pump samples in the 1.2 to 1.3 μm region. For the present study, the ability to pump only the WW and not the NW was imperative since this is how a charge density localized in the WW was generated. The experimental setup was a standard PL arrangement. The ADQW sample was mounted in a closed-cycle helium cryostat and held at a constant temperature of 8.5 K throughout the steady-state measurements. The sample was pumped by tuning the Forsterite laser to 1275 nm. The pump wavelength is between the lowest allowed transition in the NW (1238 nm) and the lowest allowed transition in the WW (1370 nm). Hence, electrons and holes are only generated in the WW. The PL from the sample was then dispersed using a 1/4-meter spectrometer and detected using a calibrated InGaAs linear diode array/OMA combination.

The measured PL spectra at various applied bias voltages are shown in Fig. 11. At zero applied bias, only one PL peak is observed corresponding to the radiative decay of free heavy-hole

excitons in the WW. As the reverse bias is increased, a small Stark shift of the PL peak to longer wavelengths is observed. When the reverse bias reaches a value of 8.0 V, the PL peak splits into two peaks. The splitting is due to the anti-crossing of electron levels, and it indicates that electrons

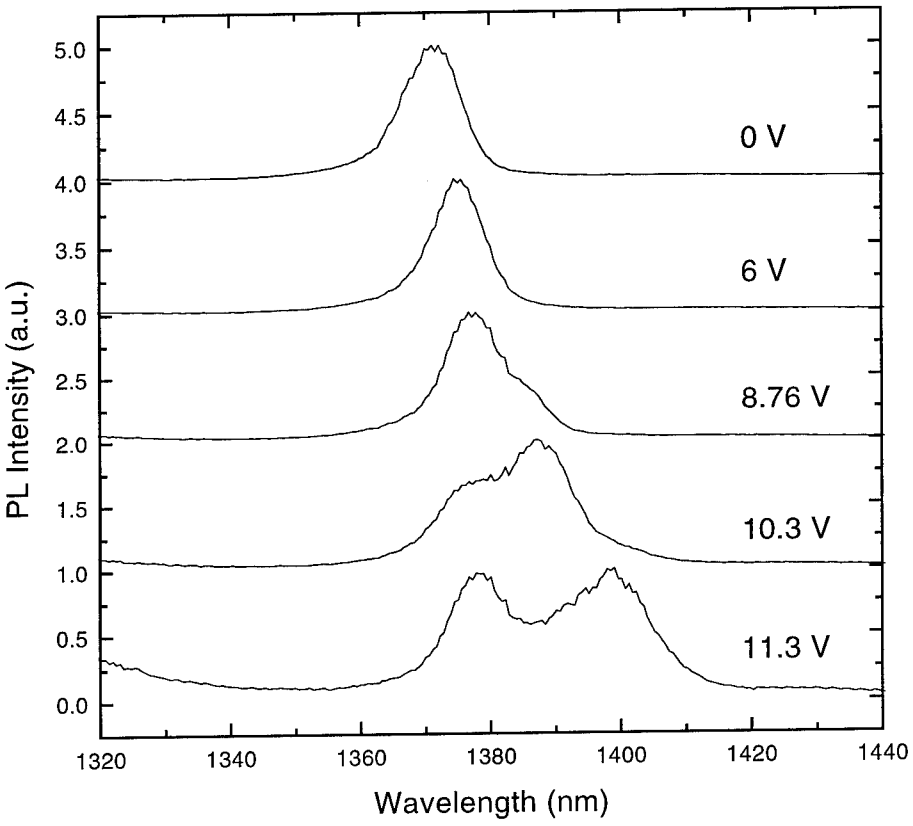

Figure 11 Time-integrated PL spectra at different applied reverse biases. The long wavelength PL peak appearing at biases greater than 8.0 V indicates strong transfer of electrons from the WW to NW.

which were highly localized in the WW at low biases are now delocalized over both the wide and narrow wells. Further evidence of the electron delocalization is seen as the reverse bias is increased. For reverse biases greater than 8.0 V, the second peak becomes clearly separated from

the initial PL peak. In fact, as the bias is increased, the second peak shows a continuous shift to longer wavelengths. The long wavelength peak originates from the spatially-indirect transition (cross-transition) between electrons localized in the NW and holes localized in the WW. It should be noted that the matrix element for the cross-transition is small due to the spatially localized envelope wavefunctions of the electrons and holes. Hence, the density of transferred electrons must be large in order for a relatively large PL signal at this transition energy to be present.

Figure 12 shows the evolution of the PL peaks as a function of reverse bias for different pump powers. At the lowest pump power, the single peak splits into two peaks at a reverse bias of

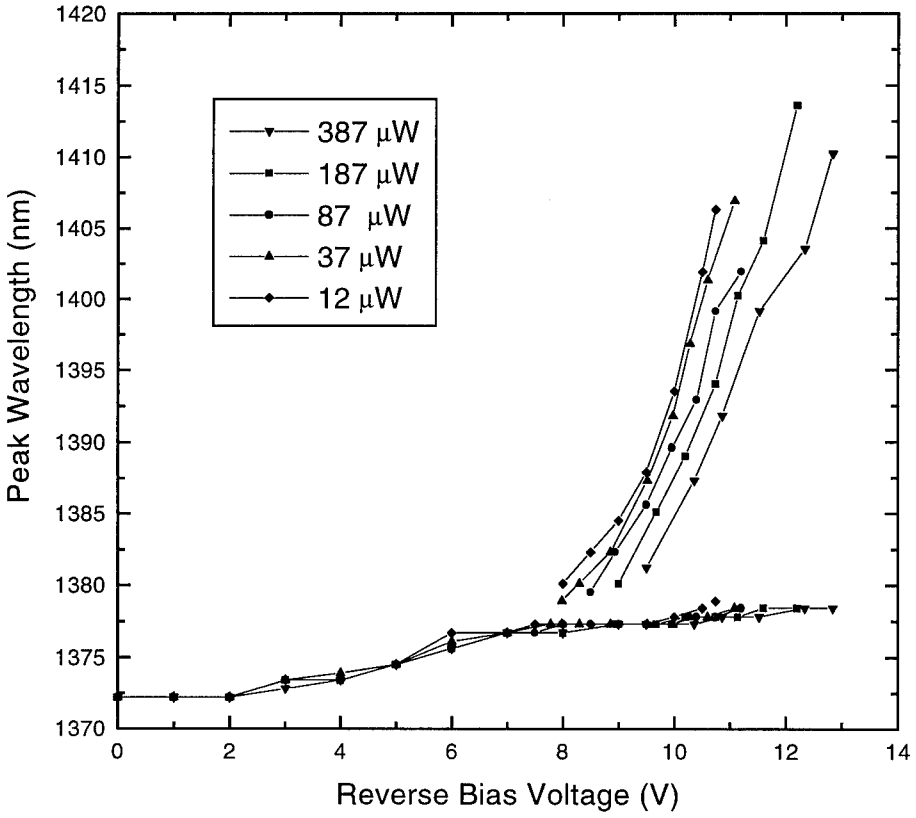

Figure 12 PL peak positions as a function of applied reverse bias for various pump intensities showing the effects of space-charge buildup.

approximately 8.2 V. As expected, the long wavelength peak originating from the cross-transition continuously shifts to longer wavelengths as the applied bias increases. The energy of this transition is a linear function of the applied field since the relative shift between these two levels has a linear field. An interesting effect is observed as the pump power is increased. For increased pump intensities, the bias voltage at which the cross-transition splits off increases due to the build-up of a space-charge field which screens the applied field. The space-charge field results from the spatial separation of electrons and holes localized in the narrow and wide wells, respectively.[43]

The results of the PL experiment demonstrate the ability to control the spatial location of photo-induced electrons in the (Ga,In)As/(Al,In)As ADQW structure through the use of an external bias. In the next section, an electro-optic modulator is described which takes advantage of the ability to control the spatial position of electrons to enhance the electro-optic properties of (Ga,In)As/(Al,In)As ADQWs at near-IR wavelengths.

We designed an ADQW structure in which an excess conduction band electron density is intentionally formed by selectively doping the wide-well (WW) n-type as shown in Fig. 13(a). The presence of excess electrons bleaches the absorption near the bandedge of the WW. The lowest energy transition in the WW is thus given by

$$\hbar\omega = E_{\mu=0} + \mu_e(F) + E_{\|}^{v} \tag{3}$$

where $E_{\mu=0}$ is the lowest energy WW transition in the absence of excess electrons, $\mu_e(F)$ is the field-dependent electron quasi-chemical potential with respect to the lowest allowed energy in the WW, and $E^{v}_{\|}$ is the in-plane hole energy required for momentum conservation. Hence, Eq. 3 indicates that the WW absorption edge will be blue-shifted with respect to the absorption edge in the absence of excess electrons, i.e. $\mu_e = 0$. An electric field applied perpendicular to the plane of

the quantum wells will reduce the energy separation between the lowest electron levels in the wide and narrow wells as shown in Fig. 13(b). As a result, the excess electrons localized in the WW can tunnel to the narrow well (NW) via real space electron transfer. The transfer of the electrons reduces μ_e resulting in the recovery of the absorption near the WW bandedge and causing an apparent red-shift of the WW absorption edge.

To experimentally demonstrate the enhanced electroabsorption properties of the structure, a doped 50/35/70 ADQW structure was grown by molecular beam epitaxy on n-type (100) InP substrates. The electrical bias was applied via an *n-i-n* diode consisting of a 0.35 μm layer of n-type $Ga_{0.3}Al_{0.18}In_{0.52}As$ (Si, $2x10^{18}$ cm^{-3}) followed by a 0.865 μm intrinsic region and capped with a 0.2 μm layer of n-type $Ga_{0.3}Al_{0.18}In_{0.52}As$ (Si, $2x10^{18}$ cm^{-3}). The intrinsic region consisted of 30 periods of 100 Å $Al_{0.48}In_{0.52}As$ barrier/ 70 Å $Ga_{0.47}In_{0.53}As$ wide well doped n-type over the central 40 Å (Si, $1x10^{12}$ cm^{-2})/ 35 Å $Al_{0.48}In_{0.52}As$ tunnel barrier/ 50 Å $Ga_{0.47}In_{0.53}As$ narrow well all between two layers of 500 Å undoped $Al_{0.48}In_{0.52}As$. The diodes were processed into 150 μm diameter mesa diodes with ring top contacts to allow optical transmission experiments. The modulator sample was mounted in a closed-cycle helium cryostat and held at a temperature of 50 K.

The measured absorbance spectra at bias fields of 0 and 74 kV/cm, corresponding to applied voltages of 0 and 6.4 V, respectively, are shown in Fig 14. The peaks in the zero-field spectrum are the light- and heavy-hole excitonic absorption features associated with the lowest energy transition in the NW. The excitonic features associated with the WW, however, are completely bleached by the presence of the excess electron density. In fact, due to bandfilling in the first WW electron subband, the WW absorption is bleached to wavelengths approaching the NW bandedge. With the applied field present, the absorption associated with the WW recovers

while the absorption associated with the NW becomes bleached. It should be stressed that the observed changes are not due to the QCSE. In undoped (Ga,In)As/(Al,In)As coupled quantum well systems consisting of similar well widths, excitonic absorption features persist to much higher

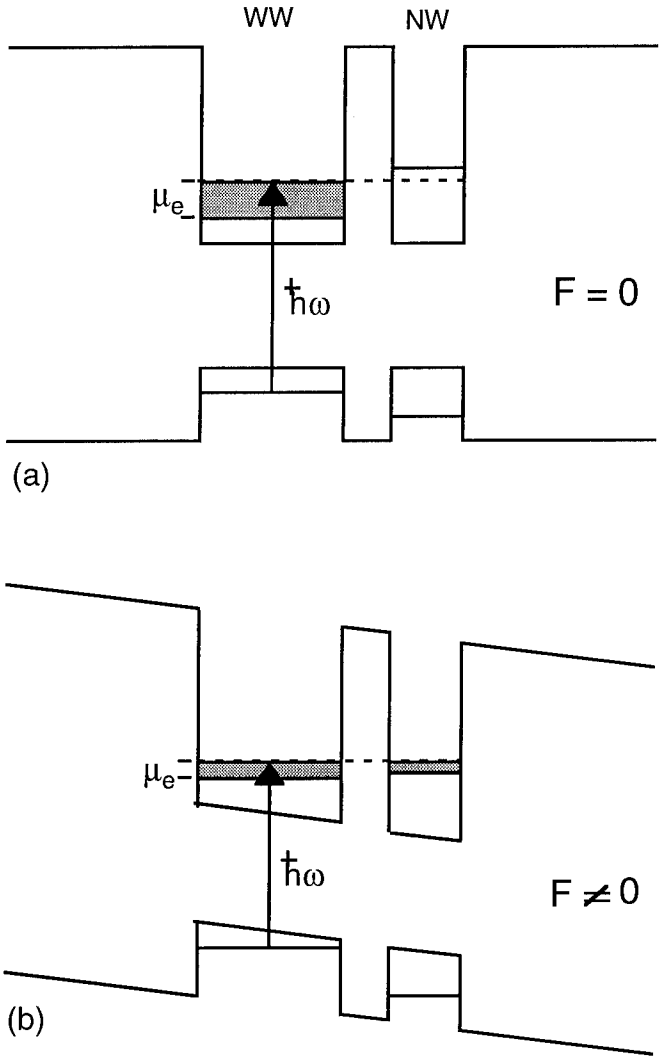

Figure 13 Conduction and valence band structure of the doped ADQW modulator in the (a) unbiased, F = 0 and (b) biased, F ≠ 0 states. The shaped regions represent states occupied by excess electrons.

applied fields than those considered in this work.[36] Hence, the observed absorption changes can only arise from the real-space transfer of electrons from the WW to the NW.

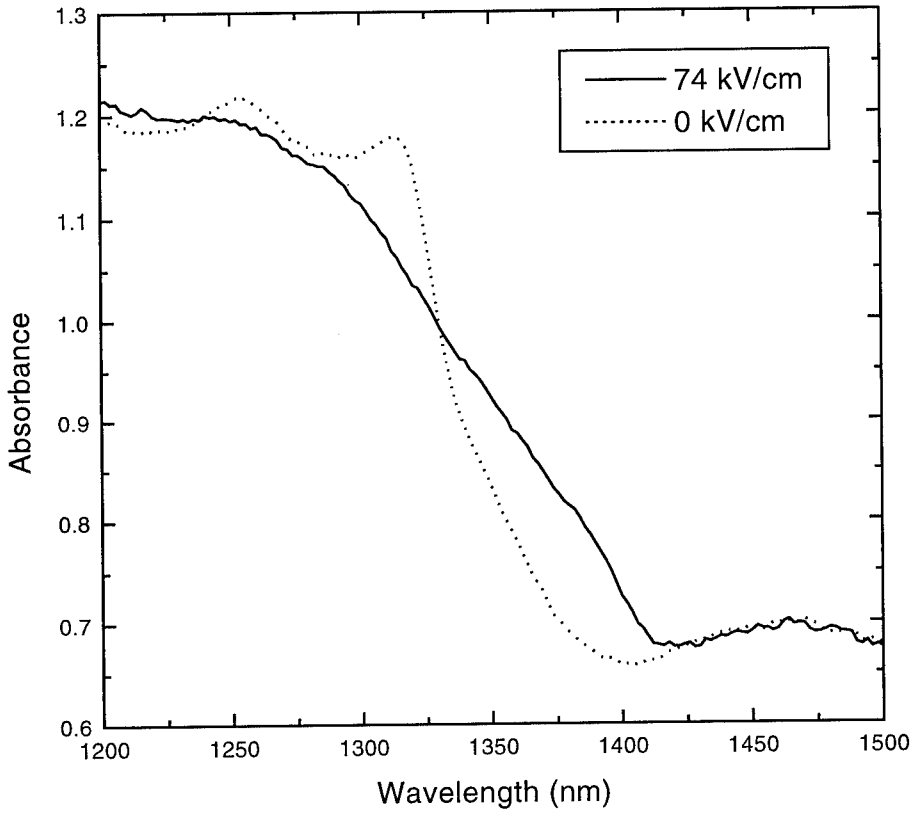

Figure 14 Measured absorbance spectra of the doped modulator for applied fields of 0 and 74 kV/cm.

The characteristics of the doped modulator were compared to the electroabsorption characteristics of the undoped 40/35/70 ADQW sample described above. Since the 35 Å tunnel barrier is relatively thick, the WW and NW are essentially uncoupled for the range of applied fields considered here. Hence, the change in the WW absorption with applied field is strictly due to the QCSE. To accurately compare the two modulators, the built-in potential of the *p-i-n* diode must be included in the total applied field for the undoped sample. The built-in potential was determined to be -1.63 V at 50 K by using a photovoltage technique.[44] In the photovoltage technique,

electrons and holes are generated above the intrinsic region bandgap by an argon-ion laser. Due to the presence of the built-in potential, the photogenerated electrons and holes are swept to the *n*- and *p*-sides of the diode, respectively. The carriers accumulate at opposite sides of the diode since the diode is left in the open-circuit configuration. The excess charge generates a space-charge field which self-consistently screens the built-in potential. The accumulation of carriers stops when the photo-induced potential is equal and opposite to the built-in potential of the diode, i.e. further increase in the laser power does not increase the measured photovoltage. The depletion region width of both diodes was assumed to be equal to the corresponding intrinsic region width. Figure 15 shows the red-shift of the bandedge as a function of applied field for both the doped (solid squares) and undoped (open squares) modulators. The red-shift was measured as the shift of the WW heavy-hole exciton absorption resonance for the undoped sample and as the shift of the peak in the $\Delta\alpha L$ spectra for the doped sample. The red-shift of the bandedge for the undoped sample is quadratic with increasing field as expected from the QCSE. However, the red-shift of the band edge exhibited by the doped sample is much larger with increasing field and has an almost linear field dependence. In fact, for an applied field of approximately 50 kV/cm (corresponding to an applied voltage of only 4.3 V) the red-shift of the doped sample is more than six times larger than the red-shift of the undoped sample. The shift of the absorption edge of the doped sample follows the red-shift of the short wavelength PL emission edge (open triangles in Fig. 15) since both are dependent on the position of the electron quasi-chemical potential with respect to the lowest allowed energy in the WW.

In conclusion, we have demonstrated a novel electroabsorption mechanism based on selective doping in ADQW structures. The modulator utilizes real space electron transfer to provide efficient absorption modulation. The electron concentration in both the wide and narrow wells was investigated using field dependent absorption and photoluminescence spectroscopy. The doped modulator exhibits a significantly larger red-shift with applied field than an undoped

structure which utilizes the QCSE. Efforts are currently underway to optimize the coupled quantum well design and diode structure for room-temperature operation.

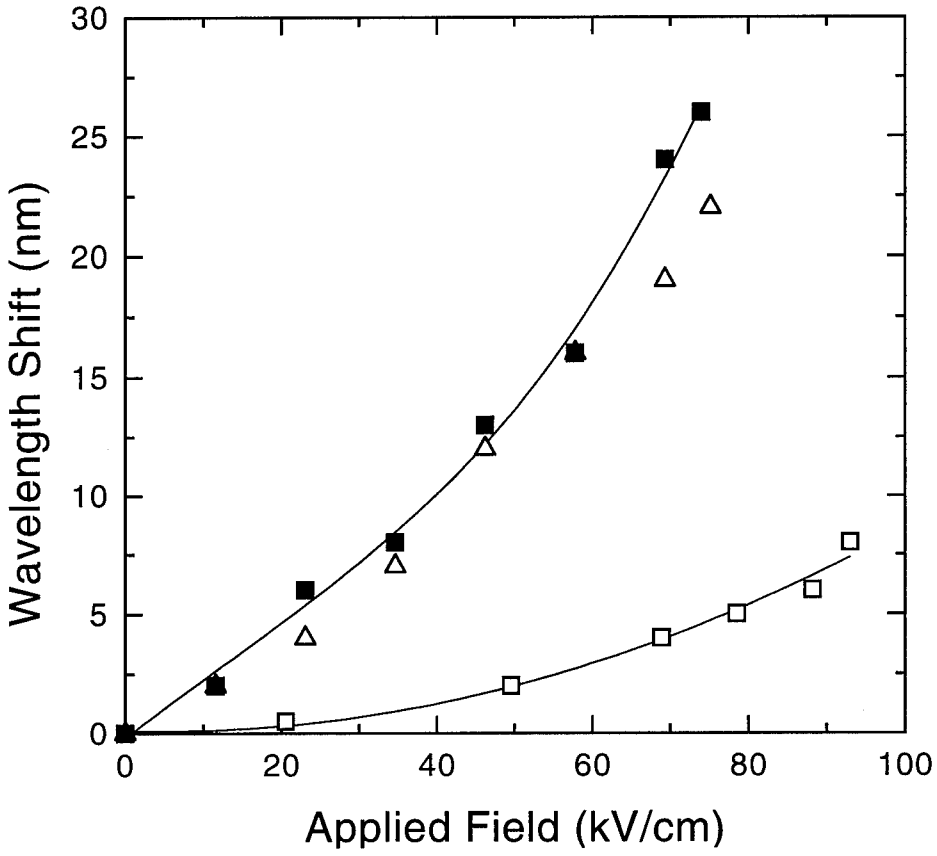

Figure 15 Comparison of the band edge shift for the doped (solid squares) and undoped (open squares) ADQW structures. The solid lines are fits to the measured data. The red shift of the short-wavelength PL edge is also shown (open triangles).

6. References

1. G. Li, R.K. Boncek, X. Wang, and D.H. Sackett, "Transient and Optoelectronic Feedback-Sustained Pulsation of Laser Diodes at 1300 nm," IEEE Photon. Technol. Lett., **7** (8), 854, (1995).
2. K.I. Kang, I. Glesk, T.G. Chang, P.R. Prucnal and R.K. Boncek, "Demonstration of all-optical Mach-Zehnder demultiplexer," Elec. Lett., **31** (9), 749, (1995).
3. M. F. Krol, S. Ten, B. P. McGinnis, M. J. Hayduk, G. Khitrova, and N. Peyghambarian, Phys. Rev. B **52** (20) 14344 (1995).
4. M. F. Krol, R. P. Leavitt, J. T. Pham, B. P. McGinnis, and N. Peyghambarian, Appl. Phys. Lett. **66** (22) 3045 (1995).
5. T. L. Paoli and J. Ripper, "Optical pulses from cw GaAs injection lasers," Appl. Phys. Lett. **15**, 105-107 (1965).
6. J. P. van der Aiel, J. L. Merz, and T. L. Paoli, "Study of intensity pulsations in proton-bombarded strip-geometry double-heterostructure AlxGa1-xAs lasers," J. Appl. Phys. **50** (7), 4620-4637, (1979).
7. K. D. Chik, J. C. Dyment, and B. A. Richardson, "Self-sustained pulsations in semiconductor lasers: experimental results and theoretical confirmation," J. Appl. Phys. **51** (8), 4029-4037, (1980).
8. M. Ueno and R. Lang, "Conditions for self-sustained pulsation and bistability in semiconductor lasers," J. Appl. Phys. **58** (4), 1689-1692 (1985).
9. P. E. Barnsley, H. J. Wickes, G. E. Wickens, and D. M. Spirit, "All-optical clock recovery from 5 Gb/s RZ data using a self-pulsating 1.56 mm laser diode," IEEE Photon. Technol. Lett. **3**(10), 942-945 (1991).

10. X. Wang and Guifang Li, "Generating microwave/millimeter wave frequency modulation by laser diode self-sustained pulsation," SPIE Proceeding, vol. **1703**, 163-175 (1992).

11. X. Wang, Guifang Li and C. S. Ih, "Microwave/millimeter-wave frequency subcarrier lightwave modulations based on self-sustained pulsation of laser diodes," IEEE J. Lightwave Technol. **LT-11**(2), 309-315 (1993).

12. J. B. Georges and K. Y. Lau, "800 Mb/s microwave FSK using a self-pulsating compact disk laser diode," IEEE Photon. Technol. Lett. **4**(6), 662-665 (1992).

13. J. B. Georges and K. Y. Lau, "Self-pulsating laser diodes as fast-tunable (<1ns) FSK transmitters in subcarrier multiple-access networks," IEEE Photon. Technol. Lett. **5**(2), 242-245 (1993).

14. P. Hill and R. Olshansky, "Twenty channel FSK subcarrier multiplexed optical communication system for video distribution," Electron. Lett., **24**(14), 892-893 (1988).

15. D. Lenstra, B. H. Verbeek, and A. J. den Boef, "Coherence collapse in single-mode semiconductor lasers due to optical feedback," IEEE J. Quantum Electron. **QE-21** (6), 674-679 (1985).

16. H. A. Haus, "Parameter ranges for CW passive mode locking," IEEE J. Quantum Electron. **QE-12** (3), 169-176 (1976).

17. R.K. Boncek, P.R. Prucnal, M.F. Krol, S.T. Johns and J.L. Stacy, "Five gigabit/second operation of a 50-channel optical time-division multiple-access interconnect," Opt. Engineering, **31** (11), 2442 (1992).

18. J.P. Sokoloff, P.R. Prucnal, I. Glesk, and M. Kane, IEEE Photon. Technol. Lett., **5** (7), 787 (1993).

19. S. Nakamura, K. Tajima, and Y. Sugimoto, Appl. Phys. Lett., **65** (3), 283 (1994).

20. K.I. Kang, T.G. Chang, I. Glesk, P.R. Prucnal and R.K. Boncek, "Demonstration of ultrafast, all-optical, low control energy, single wavelength, polarization independent, cascadable, and integratable switch," Appl. Phys. Lett., **67** (5), 605 (1995).

21. J. Shah in *Optics of Semiconductor Nanostructures*, edited by F. Henneberger, S. Schmitt-Rink, and E. O. Göbel (Akademie Verlag, Berlin, 1993) pp. 149.

22. M. G. W. Alexander, W. W. Rühle, R. Sauer, and W. T. Tsang, Appl. Phys. Lett. **55** (9) 885 (1989).

23. S. Muto, T. Inata, A. Tackeuchi, Y. Sugiyama, and T. Fujii, Appl. Phys. Lett. **58** (21) 2393 (1991).

24. B. Deveaud, A Chomette, F. Clerot, P. Auvray, A. Regreny, R. Ferreira, and G. Bastard, Phys. Rev. B **42** (11) 7021 (1990).

25. D. Y. Oberli, J. Shah, T. C. Damen, J. M. Kuo, J. E. Henry, J. Lary, and S. M. Goodnick, Appl. Phys. Lett. **56** (13) 1239 (1990).

26. R. Ferreira and G. Bastard, Europhys. Lett. **10** (3) 279 (1989).

27. T. B. Norris, N. Vodjdani, B. Vinter, E. Costard, and E. Böckenhoff, Phys. Rev. B **43** (2) 1867 (1991).

28. Ph. Roussignol, A. Vinattieri, L. Carraresi, M. Colocci, and A. Fasolino, Phys. Rev. B **44** (16) 8873 (1991).

29. R. Sauer, K. Thonke, and W. T. Tsang, Phys. Rev. Lett. **61** (5) 609 (1988).

30. J. Shah, IEEE J. Quan. Elec. **24** (2) 276 (1988).

31. R. Strobel, R. Eccleston, J. Kuhl, and K. Köhler, Phys. Rev. B **43** (15) 12564 (1991).

32. R. Ferreira and G. Bastard, Phys. Rev. B **40** (2) 1074 (1989).

33. R. P. Leavitt and J. L. Bradshaw, J. Appl. Phys. **76** (6) 3429 (1994).

34. C. Tanguy, B. Deveaud, A. Regreny, D. Hulin, and A. Antonetti, Appl. Phys. Lett. **58** (

35. A. Tackeuchi, S. Muto, T. Inata, and T. Fujii, Appl. Phys. Lett. **58** (15) 1670 (1991).

36. R. P. Leavitt, J. W. Little, and S. C. Horst, Phys. Rev. B **40** (6) 4183 (1989).

37. M. Wegener, T. Y. Chang, I. Bar-Joseph, J. M. Kuo, and D. S. Chemla, Appl. Phys. Lett. **55** (6) 583 (1989).

38. N. Vodjdani, B. Vinter, V. Berger, E. Böckenhoff, and E. Costard, Appl. Phys. Lett. **59** (5) 556 (1991).

39. Y. J. Ding, C. L. Guo, S. Li, J. B. Khurgin, K. K. Law, J. Stellato, C. T. Law, A. E. Kaplan, L. A. Coldren, Appl. Phys. Lett. **59** (9) 1025 (1991).

40. C.C. Hsu, B.P. McGinnis, J.P. Sokoloff, G. Khitrova, H.M. Gibbs, N. Peyghambarian, S.T. Johns, and M.F. Krol, J. Appl. Phys. **70** (10) 5615 (1991).

41. M. F. Krol, T. Ohtsuki, G. Khitrova, R. K. Boncek, B. P. McGinnis, H. M. Gibbs, and N. Peyghambarian, Appl. Phys. Lett. **62** (13) 1550 (1993).

42. R. P. Leavitt and J. L. Bradshaw, J. Appl. Phys. **76** (6) 3429 (1994).

43. R. Sauer, K. Thonke, and W. T. Tsang, Phys. Rev. Lett. **61** (5) 609 (1988).

44. J. L. Bradshaw, R. P. Leavitt, J. T. Pham, and F. J. Towner, Phys. Rev. B **49** (3) 1882 (1994).

7. Acknowledgment

The authors would like to acknowledge Guifang Li and David Sackett from the Rochester Institute of Technology for their work on the self-sustained pulsation of semiconductor laser diodes.

Koo Il Kang, Ivan Glesk and Paul Prucnal from Princeton University for their work on the development of the colliding pulse Mach Zehnder modulator. These experiments were performed entirely at Princeton University.

N. Peyghambarian from the University of Arizona and R. P. Leavitt from the Army Research Laboratory in Adelphi, MD for their contributions to the work on the ultrafast tunneling experiments and electroabsorption modulator, and Dr. H. M. Gibbs from the University of Arizona for many fruitful discussions concerning the tunneling experiments.

☆U.S. GOVERNMENT PRINTING OFFICE: 1996-710-126-20196

MISSION

OF

ROME LABORATORY

Mission. The mission of Rome Laboratory is to advance the science and technologies of command, control, communications and intelligence and to transition them into systems to meet customer needs. To achieve this, Rome Lab:

a. Conducts vigorous research, development and test programs in all applicable technologies;

b. Transitions technology to current and future systems to improve operational capability, readiness, and supportability;

c. Provides a full range of technical support to Air Force Materiel Command product centers and other Air Force organizations;

d. Promotes transfer of technology to the private sector;

e. Maintains leading edge technological expertise in the areas of surveillance, communications, command and control, intelligence, reliability science, electro-magnetic technology, photonics, signal processing, and computational science.

The thrust areas of technical competence include: Surveillance, Communications, Command and Control, Intelligence, Signal Processing, Computer Science and Technology, Electromagnetic Technology, Photonics and Reliability Sciences.